Geometric Resonances for High-Sensitivity Microfluidic Lasing Sensors

W. Morrish,[1] N. Riesen,[2,3] S. Stobie,[1] A. François,[2,3] and A. Meldrum[1,*]

[1]*Department of Physics, University of Alberta, Edmonton, Alberta T6G2E1, Canada*

[2]*School of Engineering, University of South Australia, Mawson Lakes, South Australia 5095, Australia*

[3]*The Institute for Photonics and Advanced Sensing, School of Physical Sciences, University of Adelaide, Adelaide, South Australia 5005, Australia*

Microcapillaries are inherently fluidic sensing platforms that can, under appropriate conditions, support lasing. We propose and demonstrate a lasing microcapillary sensor based on "star" and "triangle" interferences arising from reflection and refraction at the inner and outer microcapillary walls. These interferences lead to distinct modal trajectories that sample the channel medium inside the microcavity structure. Both star and triangle resonances are therefore sensitive to the nature of the channel medium, yielding theoretical and experimental sensitivities significantly exceeding those found for sensors based on conventional whispering-gallery modes. Additional enhancement can be achieved because the two main resonance families shift in an opposite sense, yielding a differential sensitivity that can reach several thousand nanometers per refractive index "unit." These devices represent a robust, yet easily fabricated optical sensor and capillary-based lasing system for microfluidic sensing.

I. INTRODUCTION

Microcavity resonators are a natural fit for sensing applications. They are compact and can measure changes in humidity [1], temperature [2], and force [3]. They can measure chemical reactions [4] and can be functionalized to detect specific proteins [5], DNA [6], viruses [7], and individual nanoparticles [8]. Microcapillaries also provide an intrinsic flow-through capability, whereas other geometries, such as microspheres, disks, and fiber-based resonators, require more-complicated external channels and sampling chambers.

Two main capillary-type microcavity sensors have been proposed. Liquid-core-optical-ring-resonator sensors (LCORRS) are capillaries whose walls have been thinned below 5 μm [9]. Light is then coupled into the whispering-gallery modes (WGMs) through the use of a phase-matched waveguide or fiber taper, which requires submicron positioning apparatus and/or a narrow-bandwidth tunable laser. LCORRS are also fragile and their fabrication can require injection and pumping of hydrofluoric acid.

Fluorescent-core microcavities (FCMs) are standard thick-walled microcapillaries with a high-refractive-index fluorescent layer on the inside of the capillary channel [10]. The WGMs can be observed in the fluorescence emitted from the channel coating. While FCMs are more robust and

easier to prepare, their drawbacks include low light levels, low Q factors of typically 1000, and relatively low refractometric sensitivity [11]. While lasing FCMs can alleviate the first two issues to some degree [12], the lasing is subject to photobleaching and does not increase the sensitivity.

LCORRSs and FCMs typically have sensitivities (S) of 5–30 nm per refractive index "unit" (RIU), although the high-order radial modes can reach 200 nm/RIU [13] or 570 nm/RIU [14], respectively. A sensitivity of 967 nm/RIU was achieved in capillary resonators having a layered structure with outwardly decreasing refractive indices [15]. Surface-plasmon resonators typically show comparatively lower sensitivities [16]; whereas Fabry-Perot cavities [17,18] and photonic crystals [19] can achieve values near 1000 nm/RIU. Specially designed devices such as coupled optofluidic ring lasers can reach even higher values [20]. The detection limit for refractometric devices is generally defined as $L_d = R_e/S$, where R_e is the "resolution" of the sensor, which is based on the noise present in a given configuration [21]. For capillaries, the detection limit ranges from 10^{-4} to 10^{-6} RIU depending on the geometry. Surface-plasmon sensors can routinely achieve detection limits of 10^{-6} RIU [16], the detection limits of Fabry-Perot cavities range from 10^{-4} to 10^{-6} RIU [17,18], and the detection limit of optofluidic ring lasers reaches 10^{-7} RIU [20].

Here we demonstrate a novel lasing capillary sensor that is both robust and sensitive by using geometric modes in the lasing regime. We start by analyzing the trajectories

*ameldrum@ualberta.ca

of these modes and derive an equation for their sensitivity. We then fabricate devices, characterize the resonances, and measure the sensitivity experimentally. We find two families of lasing modes that shift in an opposite sense as a function of the analyte refractive index, reaching sensitivities significantly greater than those of other capillary-based devices.

II. THEORY

There are two types of resonance that can be supported. In the first type, light travels around the full circumference of the capillary, periodically refracting into the glass wall [Fig. 1(a)]. If the path difference after one round trip is an integer number of wavelengths, a "star-mode" resonance will form. These modes require that the refracted ray approaches the outer boundary at an angle larger than the critical angle. The resonant wavelengths obtained by geometric analysis are

$$\lambda_{\text{TE,TM}} = \frac{2N}{m - N(\phi_{\text{TE,TM},2}/2\pi)} \left(\frac{Rn_2^2 \sin\alpha}{n_1 \cos\psi} + rn_1 \sin\psi \right),$$
(1)

where λ is the mode wavelength, order N represents the number of points on the star, m is the mode number (i.e., the number of wavelengths in the optical path), $\phi_{\text{TE,TM},2}$ is the phase change on total internal reflection at surface 2 for TE- or TM-polarized modes, R is the outer radius of the capillary, r is the inner radius of the capillary, n_1 is the refractive index inside the channel, n_2 is the refractive index of the glass wall, α is the half-angle subtended by the points of incidence for the ray that refracts into the glass wall and returns to surface 1 [Fig. 1(c), line ABC], and ψ is the half-angle subtended by the path that reflects through the channel [Fig. 1(a), line AC]. The phase shifts on internal reflection from surface 2 are calculated from the Fresnel equations.

The star modes have the constraint that $N(\psi + \alpha) = \pi$, establishing a limit on the possible values of N. For example, in capillaries with $n_1 = 1.348$, a 125-μm inner radius, and a 160-μm outer radius, the only allowable values of N are integers 5–8. To find the resonant wavelengths, we write the angle α in terms of the other parameters:

$$\alpha = \sin^{-1}\left(\frac{n_1}{n_2} \cos\psi \right) - \sin^{-1}\left(\frac{rn_1}{Rn_2} \cos\psi \right). \quad (2)$$

Pairs of angles ψ and α can be calculated by solving Eq. (2) numerically, and then the resonant wavelengths can be calculated from Eq. (1).

The sensitivity of the star modes can be determined by taking the derivative of Eq. (1) with respect to n_1 for either polarization. We focus on the TE case (i.e., electric field parallel to the capillary axis), although the TM
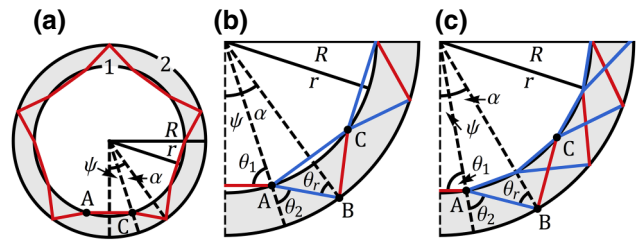

FIG. 1. Ray diagrams showing possible resonance configurations. Inner and outer capillary surfaces are labeled 1 and 2, respectively, θ_2 is the angle of refraction after light enters the glass wall, and θ_r is the angle of reflection at surface 2. Other symbols are defined after Eq. (1). (a) A ray reflects off the glass-air interface five times. (b),(c) An incoming ray is split into two paths via Fresnel reflection and recombines after either one reflection (b) or two reflections (c) of the internal ray.

result is similar. Since many of the variables in Eq. (1) are themselves dependent on n_1, the derivative has no simple analytical solution. We therefore solve $d\lambda/dn_1$ numerically, finding sensitivities up to 350 nm/RIU for capillaries with the largest r/R ratio, as shown in Fig. 2(a). In general, star-mode sensitivities decrease with increasing orders, while sensitivity increases as the r/R ratio increases.

In the second type of resonance, a wave propagating through the capillary channel is incident on the glass wall, splits into a reflected and refracted component at point A, and recombines again at point C [Figs. 1(b) and 1(c)]. If these rays interfere in phase, they form a "triangle" resonance. Building upon a simpler analysis [22], we find the condition for a triangle is

$$\lambda_{\text{TE,TM}} = \frac{2 \left(v \frac{Rn_2^2 \sin\alpha}{n_1 \cos\psi} - urn_1 \sin\psi \right)}{m - v \frac{\phi_{\text{TE,TM},2}}{2\pi} - u \frac{\phi_{\text{TE,TM},1}}{2\pi}}, \quad (3)$$

where u and v are integers such that $u\psi = v\alpha$, and the phase shifts on reflection at surface 1 are $\phi_{\text{TE},1} = \pi$ and $\phi_{\text{TM},1} = 0$
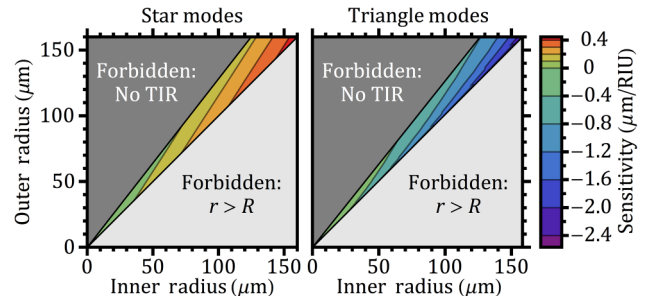

FIG. 2. Theoretical sensitivities of the TE-polarized modes for inner and outer capillary radii up to 160 μm. Failure of total internal reflection (TIR) due to the small angle of incidence prevents lasing in the upper "forbidden" regions. The lower forbidden region has inner radius exceeding the outer radius.

when $\sin^{-1}(\cos\psi) < \tan^{-1}(n_2/n_1)$ and π otherwise. In the case of $u = v$ [i.e., when the two angles are the same as in Fig. 1(c)],

$$\psi = \arccos\left[\frac{1}{12rRn_1^2}(2w - w^2zy^{-1/3} - y^{1/3}z*)\right], \quad (4)$$

where $w = r^2n_1^2 + R^2n_1^2 + R^2n_2^2$, $x = 9r^2R^4n_1^4n_2^2$, $y = w^3 - -6x + (36x^2 - -12w^3x)^{0.5}$, and $z* = 1 - 3^{0.5}i$.

When $u = 1$, the inner ray path goes straight from point A to point C; if $u = 2$, there is an additional inner-wall reflection [Fig. 1(c)]. If $v = 2$, then there are two outer-wall reflections, making a "double-triangle" mode. The triangle-mode sensitivity is the derivative of Eq. (3) with respect to n_1. When $u = v$, the sensitivity is negative and larger than for the star modes [Fig. 2(b)], reaching thousands of nanometers per RIU for increasing r/R ratio. The star and triangle modes can also be coupled (i.e., they can have the same resonant wavelength) as in the experiment to follow.

For both the star and the triangle modes, total internal reflection must occur at surface 2. This places a lower cut-off for the ratio of the inner radius and outer radius of approximately 0.75 for the refractive indices used in the experimental demonstration, although it weakly depends on the mode orders N (star modes) or u and v (triangle modes). There is technically no upper limit to the radius ratio, although eventually one returns to the situation in which the mode spectrum is dominated by the WGMs, which are formed by reflections at surface 2 only.

The free spectral range (FSR) generally defines the dynamic range that can be achieved in a sensing experiment. The star-mode FSR is

$$\Delta f_{\text{star}} = \frac{cn_1\cos\psi}{2N(Rn_2^2\sin\alpha + rn_1^2\sin\psi\cos\psi)}, \quad (5)$$

whereas for triangle modes

$$\Delta f_{\text{triangle}} = \frac{cn_1\cos\psi}{2\left(vRn_2^2\sin\alpha + urn_1^2\sin\psi\cos\psi\right)}. \quad (6)$$

The star modes have a small spacing, similar to WGMs for capillaries of the same size, where $\Delta f_{\text{WGM}} = c/(2\pi Rn_2)$ and c is the speed of light. $\Delta f_{\text{triangle}}$ is approximately 20 times larger than Δf_{star}, implying a larger range relative to the sensitivity.

III. EXPERIMENTAL METHODS

Test devices are prepared from standard 125-μm-inner-radius and 160-μm-outer-radius fused-silica microcapillaries ($n \approx 1.458$ at 600 nm [23]). The polyimide coating is removed by ashing under flowing oxygen in a tube furnace at 923 K. The inner and outer radii are modified by
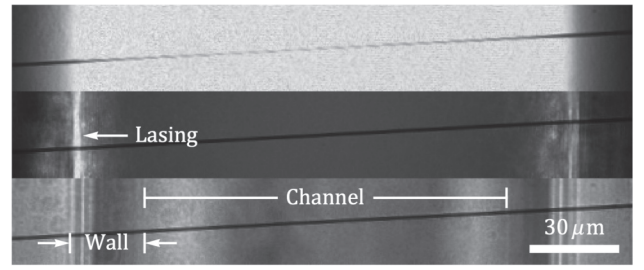

FIG. 3. Optical images of a vertically oriented capillary with radius ratio of 69:91 filled with 1 mM aqueous Rhodamine B under 532-nm cw-laser illumination (upper) and under 500-nm pulsed-laser illumination (middle), and an empty capillary under white light (lower). The black line is the spectrometer entrance slit.

heating the capillaries with a graphite filament and gently pulling them until they reached the desired radius. The r/R ratios are 52:71, 69:91, 84:114, 99:134, and 121:161 as estimated by optical microscopy (Fig. 3). Each capillary is connected to polytetrafluoroethylene tubing and affixed to a stage mounted above an objective lens. The test analyte is 1 mM Rhodamine B dissolved in aqueous solutions of either 10 or 11 wt% sucrose ($n_1 = 1.3478$ and 1.3494 at 600 nm, respectively [24]), which are pumped through the tubing and into the capillary channel with a syringe pump. The capillaries are illuminated with a Photon Technology GL-302 dye laser (500 nm, 3 Hz, pulse length approximately 1 ns), and the emission is measured with an imaging spectrometer. The mode shifts are determined by Fourier analysis [25].

IV. RESULTS AND DISCUSSION

The spectra show a set of periodic, narrowly spaced modes for the various radius ratios examined (Fig. 4). The narrowness of these modes combined with the threshold behavior is indicative of lasing. Below the threshold, no modes are visible in the spectrum because the fluorescence is dominated by the bulk fluid in the channel. For the star modes, the calculated FSR is 0.27 nm, in close agreement with the 0.26-nm spacing between adjacent lasing modes for radius ratio 121:161. With this identification, the Q factors for the star modes increase with capillary radius, ranging from approximately 3800 for the smallest capillaries to approximately 6000 for the largest as measured by dividing the central wavelength of a peak by its full width at half maximum. The triangle modes have a much larger calculated spacing of 5.9 nm, approximately consistent with the experimental results shown in Fig. 4, in which the envelope mode spacing is approximately 5.4 nm (i.e., the spacing between the groups of lasing modes). The width of the triangle-mode envelope and the underlying star-mode structure do, however, make it hard to measure the triangle-mode FSR, possibly explaining the difference
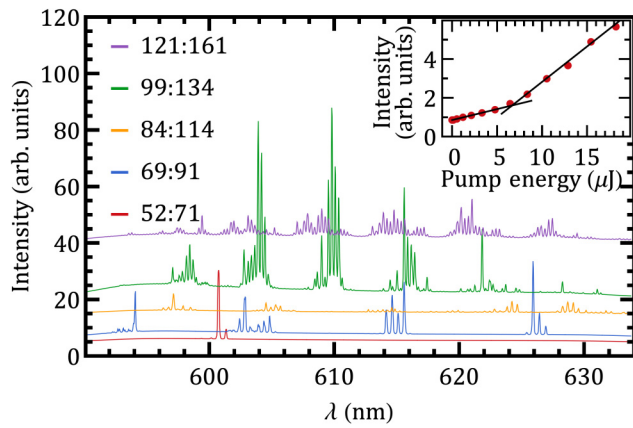
FIG. 4. Lasing spectra for capillaries of various inner and outer radii given in micrometers. The groups of lasing peaks are star modes modulated by a triangle-mode envelope. Only these coupled modes appear to lase. The inset shows the lasing threshold for the capillary with radius ratio of 121:161.

between the calculated and experimental values. Although the Q factor of the triangle modes is difficult to estimate due to the complicated underlying star-mode structure, the evidently low value is expected due to low reflectivity at surface 1 [22]. Additionally, a higher-order triangle mode [$u=2$; Fig. 1(c)] appears in the spectrum, with a measured FSR of approximately 5.8 nm, with a fairly large uncertainty.

The sensitivities are experimentally determined by collecting a series of spectra represented in Fig. 5. Triangle and star modes with differing modal parameters should produce a large set of peaks in the Fourier spectrum, and, indeed, a complex spectrum with several maxima is observed. Mode shifts are followed by monitoring the phases of the Fourier components that agreed with the calculated modal frequencies [Fig. 6(a)]. The phase shifts can then be recast as wavelength shifts, resulting in the sensor read-out shown in Fig. 6(b). The triangle-mode envelope shows a large blueshift and the star modes show a smaller redshift in the sensor read-out, as predicted by the theoretical analysis.

The calculated sensitivity of these modes can also be compared with the experimental values. The $R = 161$ μm capillary demonstrates sensitivities of 147 and -767 nm/ RIU for the star and triangle modes, respectively. These correspond to calculated sensitivities of 135 and -794 nm/RIU for $N = 5$ and $u = 1$, which appears to be reasonably good agreement given the experimental uncertainties. Since these two sets of modes have sensitivities of the opposite sign, they can be combined to achieve a sensitivity higher than either can provide alone. This yields a sensitivity of 914 nm/RIU experimentally and 929 nm/RIU from the theory.

The sensitivity of the other capillaries is also measured, yielding star-mode values of 111, 160, 227, and
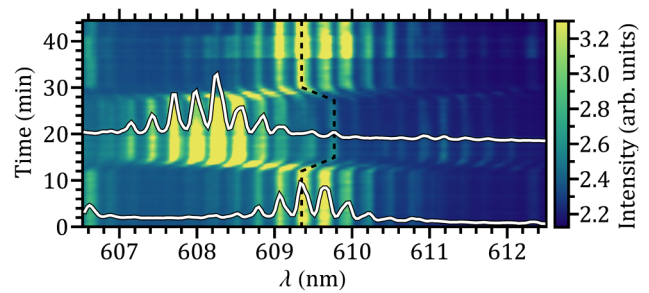

FIG. 5. Density plot illustrating a sensing run. Two spectra are overlaid in white. A 10 wt% aqueous sucrose solution is pumped through the capillary, followed by 11 wt% at approximately 12 min, and 10 wt% solution is reintroduced at approximately 28 min.

139 nm/RIU for the devices with radius ratios of 52:71, 69:91, 84:114, and 99:134, respectively. The triangle-mode sensitivities of these same capillaries are -856, -743, -828, and -991 nm/RIU, again in good agreement with the theoretical calculations described above and confirming that combined sensitivities in excess of 1000 nm/RIU can be achieved. The theory shows that even better values can be easily obtained (Fig. 2).

To calculate the detection limit, the wavelength resolution R_e is defined as 3 times the standard deviation of the data during a period where no change occurs. With
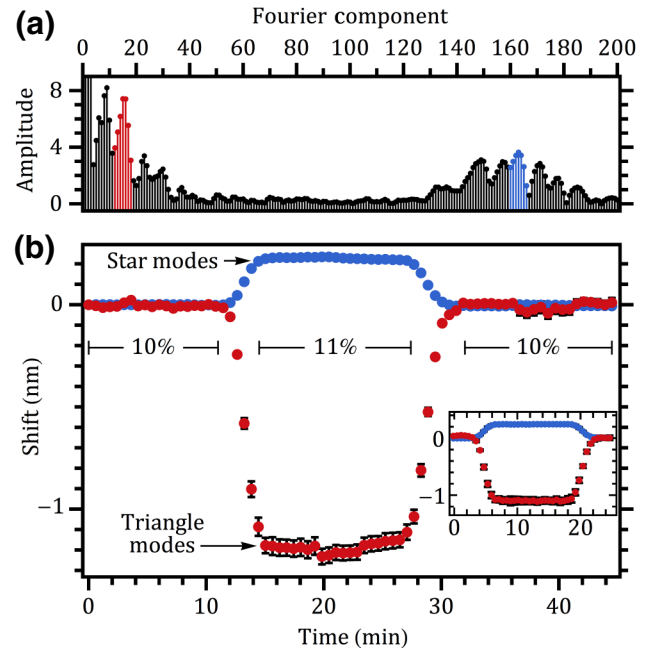

FIG. 6. (a) Discrete Fourier transform of the lasing spectrum of a capillary with 160-μm outer radius. Colors indicate the components used to create the read-out in (b). (b) Sensor read-out with 10 and 11 wt% aqueous sucrose solutions. The error bars are smaller than the data points in most cases. The inset shows the sensor read-out of the same capillary with TE polarization.

the definition $L_d = R_e/S$, the data in Fig. 6(b) yield detection limits of 3.4×10^{-5} RIU for the triangle modes and 2.5×10^{-5} RIU for the star modes. The main limitation is the jitter in the data for the triangle modes, which are harder to clearly isolate in the Fourier spectrum. In the most stable runs, however, the 3σ resolution is good enough to imply a detection limit in the mid-10^{-6} range.

Unlike WGM-based capillary lasers that rely on organic dyes in solid media [12], here the lasing modes show no bleaching over an entire experiment (i.e., 45 min). The fresh solution continuously pumped through the capillary channel minimizes oxidative effects from the excitation of triplet states common to organic chromophores. Furthermore, specific detection via surface functionalization is possible in principle, since the star and triangle modes depend on the optical properties of surface 1. The main drawback is that the fluid must contain a lasing chromophore, which may limit the range of analytes. However, this arrangement can also be desirable, such as when proteins or cells are tagged with laser dyes [26].

V. CONCLUSIONS

The star and triangle "geometric" modes of conventional microcapillaries can be used for a lasing sensor that demonstrates a combined theoretical sensitivity up to several thousand nanometers per RIU at visible wavelengths and yields a detection limit in the range from 10^{-5} to 10^{-6} RIU, depending on the stability of the experimental setup and the capillary radii. The lasing-mode structure is shown to be the result of two sets of coupled modes: closely spaced modes created as light travels in a star-shaped path around the capillary, and more-widely-spaced ones created by interference between the reflected and transmitted waves at the channel wall. The capillaries are also robust and require little preparation, thus representing an attractive option for microfluidic sensing in the lasing regime.

ACKNOWLEDGMENT

[1] A. K. Mallik, D. Liu, V. Kavungal, Q. Wu, G. Farrell, and Y. Semenova, Agarose coated spherical micro resonator for humidity measurements, Opt. Express **24**, 21216 (2016).

[2] I. Hernández-Romano, M. A. Cruz-Garcia, C. Moreno-Hernández, D. Monzón-Hernández, E. O. López-Figueroa, O. E. Paredes-Gallardo, M. Torres-Cisneros, and J. Villatoro, Optical fiber temperature sensor based on a microcavity with polymer overlay, Opt. Express **24**, 5654 (2016).

[3] T. Ioppolo, M. Kozhevnikov, V. Stepaniuk, M. V. Ötügen, and V. Sheverev, Micro-optical force sensor concept based on whispering gallery mode resonators, Appl. Opt. **47**, 3009 (2008).

[4] S. H. Huang, S. Sheth, E. Jain, X. Jiang, S. P. Zustiak, and L. Yang, Whispering gallery mode resonator sensor for in situ measurements of hydrogel gelation, Opt. Express **26**, 51 (2018).

[5] S. Lane, P. West, A. François, and A. Meldrum, Protein biosensing with fluorescent microcapillaries, Opt. Express **23**, 2577 (2015).

[6] M. D. Baaske, M. R. Foreman, and F. Vollmer, Single-molecule nucleic acid interactions monitored on a label-free microcavity biosensor platform, Nat. Nanotechnol. **9**, 933 (2014).

[7] H. Zhu, I. M. White, J. D. Suter, and X. Fan, Phage-based label-free biomolecule detection in an optofluidic ring resonator, Biosens. Bioelectron. **24**, 461 (2008).

[8] H. Li, Y. Guo, Y. Sun, K. Reddy, and X. Fan, Analysis of single nanoparticle detection by using 3-dimensionally confined optofluidic ring resonators, Opt. Express **18**, 25081 (2010).

[9] M. Sumetsky, R. S. Windeler, Y. Dulashko, and X. Fan, Optical liquid ring resonator sensor, Opt. Express **15**, 14376 (2007).

[10] C. P. K. Manchee, V. Zamora, J. W. Silverstone, J. G. C. Veinot, and A. Meldrum, Refractometric sensing with fluorescent-core microcapillaries, Opt. Express **19**, 21540 (2011).

[11] A. Meldrum, W. Morrish, S. Lane, W. Wu, T. M. Monro, and A. Francois, Luminescent capillary-based whispering gallery mode sensors: Crossing the lasing threshold, Physica Status Solidi A **215**, 1700619 (2017).

[12] A. François, N. Riesen, K. Gardner, T. M. Monro, and A. Meldrum, Lasing of whispering gallery modes in optofluidic microcapillaries, Opt. Express **24**, 12466 (2016).

[13] V. Zamora, Z. Zhang, and A. Meldrum, Refractometric sensing of heavy oils in fluorescent core microcapillaries oil gas, Sci. Technol. – Rev. IFP Energies nouvelles **70**, 487 (2015).

[14] H. Li and X. Fan, Characterization of sensing capability of optofluidic ring resonator biosensors, Appl. Phys. Lett. **97**, 011105 (2010).

[15] T. Ling and L. J. Guo, Sensitivity enhancement in optical micro-tube resonator sensors via mode coupling, Appl. Phys. Lett. **103**, 013702 (2013).

[16] M. Piliarik and J. Homola, Surface plasmon resonance (SPR) sensors: approaching their limits?, Opt. Express **17**, 16505 (2009).

[17] G. Rigamonti, M. Guardamagna, V. Bello, S. Marconi, F. Auricchio, and S. Merlo, Flow-through micro-capillary refractive index sensor based on T/R spectral shift monitoring, Biomed. Opt. Express **8**, 4438 (2017).

[18] W. Morrish, P. West, N. Orlando, E. Klantsataya, K. Gardner, S. Lane, R. Decorby, A. François, and A. Meldrum, Refractometric micro-sensor using a mirrored capillary resonator, Opt. Express **24**, 24959 (2016).

[19] F. Sun, J. Zhou, L. Huang, Z. Fu, and H. Tian, High quality factor and high sensitivity photonic crystal rectangular holes slot nanobeam cavity with parabolic modulated lat-

tice constant for refractive index sensing, Opt. Commun. **399**, 56 (2017).

[20] X. Zhang, L. Ren, X. Wu, H. Li, L. Liu, and L. Xu, Coupled optofluidic ring laser for ultrahigh- sensitive sensing, Opt. Express **19**, 22242 (2011).

[21] I. M. White and X. Fan, On the performance quantification of resonant refractive index sensors, Opt. Express **16**, 1020 (2008).

[22] H.-J. Moon and D.-Y. Kang, Strongly enhanced mode selection in a thin dielectric-coated layered microcavity laser, Opt. Lett. **32**, 1554 (2007).

[23] I. H. Malitson, Interspecimen comparison of the refractive index of fused silica, J. Opt. Soc. Am. **55**, 1205 (1965).

[24] *CRC Handbook of Chemistry and Physics*, 98th ed. (CRC Press/Taylor & Francis, Boca Raton, FL, 2017).

[25] J. W. Silverstone, S. McFarlane, C. P. K. Manchee, and A. Meldrum, Ultimate resolution for refractometric sensing with whispering gallery mode microcavities, Opt. Express **20**, 8284 (2012).

[26] Y.-C. Chen, Q. Chen, and X. Fan, Lasing in blood, Optica **3**, 809 (2016).

Correction: Equations (3) and (6) contained minor errors and have been fixed. The spacing value in the sixth sentence of Sec. IV was erroneous and has been fixed.